DIMACS Series in Discrete Mathematics
and Theoretical Computer Science
Volume **73**, 2007

Characterization of Heat-Assisted Magnetic Recording Channels

Rathnakumar Radhakrishnan, Bane Vasić, Fatih Erden, and Ching He

Abstract. The storage capacity of hard disk drives has increased tremendously over the last decade. However, the rate of increase has reached a bottle-neck as the technology approaches a theoretical limit known as the super-paramagnetic limit. Heat-Assisted Magnetic Recording (HAMR) has emerged as one of the important technologies to overcome this limit. The process of heating while writing brings about certain unique characteristics when compared to conventional schemes. In this paper, we introduce heat-assisted recording, explain the techniques used to numerically model the two-dimensional magnetization process in longitudinal HAMR and extend it to perpendicular recording. Utilizing these models, we investigate the transition characteristics that depend, among other factors, on various thermal parameters. In particular, we determine the effects of change in peak temperature and laser spot position on transition length and center.

1. Introduction

Over the last 40 years, hard drives have clearly emerged as the primary means of data storage. A basic hard drive consists of a disk made of magnetic material and a recording head. The disk is divided into many equally spaced tracks where the data is stored as a binary sequence utilizing the two directions of magnetization possible. The process of storing and retrieving information using magnetic recording is illustrated in Fig. 1. The write current to the recording head is modulated according to the information to be stored and consequently it induces a series of magnetic transitions in the medium. During the read process, magnetic transition in the medium induces a readback signal in a magneto-resistive sensor flying over it.

There have been tremendous increases in the storage capacity of hard disk drives over the last few years. Such increases were almost always achieved by scaling down the area of a bit by reducing its length and width. The medium consists of

2000 *Mathematics Subject Classification.* 68P20, 68P30, 94A40.

Key words and phrases. Heat-assisted magnetic recording, hybrid recording, transition location, transition parameter.

This work was performed as part of the INSIC HAMR ATP program with the support of the U.S. Department of Commerce, National Institute of Standards and Technology, Advanced Technology Program, Cooperative agreement number 70NANB1H3051.

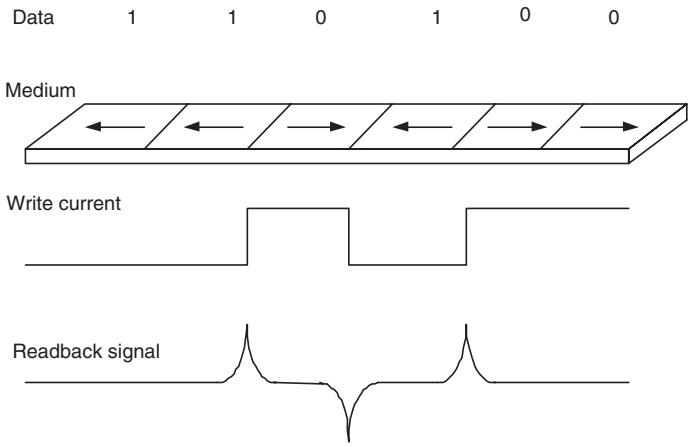

FIGURE 1. Illustration of write and read process in a magnetic recording drive

tiny magnetic particles whose volume needs to be correspondingly scaled down to maintain sufficient signal-to-noise ratio. The anisotropy energy of a grain is defined as $E_a = K_u V$, where K_u is the anisotropy of the grain and V its volume. Since anisotropy energy determines the particle stability; scaling down the volume of magnetic particles reduces their stability. The magnetic industry has reached a critical point where the particle size can no longer be reduced. This is known as the super-paramagnetic limit. The use of a high anisotropic medium to counter this problem makes it difficult to magnetize. Therefore, in order to further increase the areal density, radically new technologies need to be adopted. In this regard, Heat-Assisted Magnetic Recording (HAMR) was proposed as a very attractive option [**1**] where, a high anisotropy medium is heated by a laser at the location of transition during the write process. It is believed that it is possible to achieve an areal density of 1 terabits per square inch ($\mathrm{Tb/in^2}$) with this technology.

In order to exploit the enormous potential of HAMR, there are many challenges that need to be resolved. It is important to study and analyze the system, so as to identify and understand its characteristics. In this paper we introduce HAMR, explain the numerical models used to analyze the system and illustrate some of its important characteristics. The paper is organized as follows. Section 2 describes the principle of heat-assisted magnetic recording. Section 3 introduces the thermal Williams-Comstock model, which is shown to represent a HAMR system appropriately by incorporating all thermal and magnetic properties. Using this model, we show how to determine the magnetic transition characteristics for a given system. Further, in order to accurately capture the effects of finite-width magnetic tracks, we utilize microtrack model described in Section 4. These models enable us to characterize HAMR, especially their dependence on the thermal profile, which is illustrated in Section 5. Finally, we conclude the paper in Section 6.

2. Principle of Heat-Assisted Magnetic Recording

In heat-assisted magnetic recording, during the write process the magnetic media is heated by a laser attached to the write-head assembly. After magnetizing, the

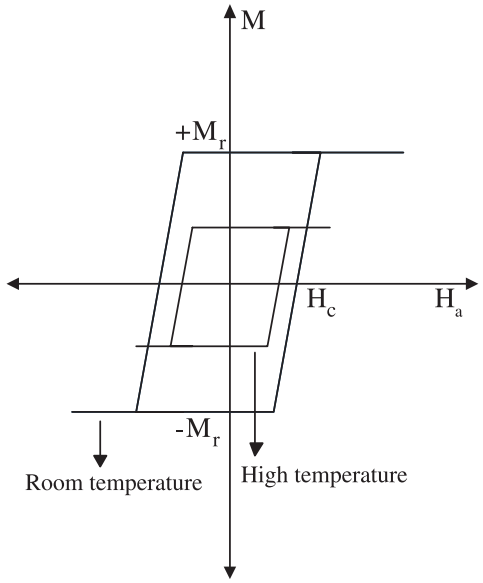

FIGURE 2. Example of an MH loop, illustrating its dependence on temperature

medium is rapidly cooled down to room temperature. The resultant magnetization of the medium is determined by its hysteresis loop (MH loop), which shows the relationship between the applied field (H_a) and the resultant magnetization (M). An example of an MH-loop is shown in Fig. 2. For stable magnetic transitions, a certain field is applied so that even after removing the field, the medium retains a certain level of magnetization. This is called remnant magnetization (M_r). The ease of making a transition in a medium is measured by its coercivity (H_c), which is the field required to reverse the direction of magnetization. The coercivity and remnant magnetization are known to vary approximately linearly with temperature. Therefore, if a transition is written at a temperature higher than room temperature, a smaller field is required to make a transition. But, almost instantaneous cooling ensures that the medium saturates at M_r corresponding to the room temperature.

The process of heating while writing enables sharper magnetic transitions to be made on high-coercive materials, thereby achieving higher stability and areal density. The read process in HAMR is identical to that of conventional magnetic recording systems. Though the fundamental idea behind HAMR is simple, the process of rapid heating and cooling brings about a number of practical challenges. More information on these can be obtained from [**4, 5, 6**].

3. The Thermal Williams-Comstock Model

The William-Comstock model is a well-known approximate analytical model that describes the transition characteristics in a conventional magnetic recording system. In [**2**], this model was extended by incorporating thermal gradients in order to determine the transition characteristics of a longitudinal HAMR system. Specifically, this model, known as the *thermal Williams-Comstock model*, captures the effects of heating through the thermal gradients of coercivity and remnant

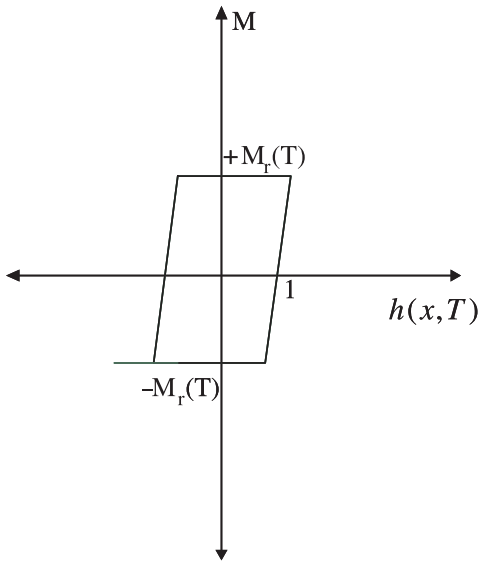

FIGURE 3. MH loop with effective field

magnetization. Application of this model to perpendicular HAMR system is also discussed in this section.

As mentioned earlier, the MH loop of a magnetic material is dependent on the temperature. In order to account for this behavior a new quantity called effective field (h) is introduced. It is defined as the ratio of applied field and coercivity,

$$h(x,T) = \frac{H_a(x)}{|H_c(T(x))|} \tag{1}$$

where $T(x)$ is the temperature profile along the direction of the movement of head (x). Note that the dependence of coercivity on temperature is shown explicitly. The new MH loop defined using h is shown in Fig. 3, where irrespective of the temperature, h is 1 at the point of reversal of magnetization. The magnetization gradient with respect to position is defined as,

$$\frac{dM}{dx} = \frac{dM}{dh}\frac{dh}{dx}. \tag{2}$$

Following a similar approach as in the Williams-Comstock model, the resultant equation, known as the *slope equation* is derived as,

$$\frac{dM(x)}{dx} = \frac{dM(x)}{dH_a}\left[\frac{dH_h(x)}{dx} + \frac{dH_d(x)}{dx} - \frac{dH_c(T)}{dT}\frac{dT}{dx}\right] \tag{3}$$

where, $M(x)$ is magnetization, H_h, H_d are the head and demagnetizing field respectively. Demagnetizing field is defined as the field from the magnetized medium, which opposes the field from the head. Note that the magnetization gradient depends on the coercivity thermal gradient.

Two quantities that completely characterize a magnetic transition are its transition center (or location) and length. Transition center is defined as the point where the magnetization of the medium reverses its direction. It occurs when the

net applied field equals the coercivity of the medium. The net applied field is defined as $H_a = H_h + H_d$. Therefore, the transition center is the solution to the equation

$$H_c(x) = H_h(x) + H_d(x) \tag{4}$$

.

Traditionally, magnetic transitions are described using an arctangent profile. Sometimes, hyperbolic tangent is argued to be better suited [**13**]. An arctangent transition is described as

$$M(x) = \frac{2M_r(T(x))}{\pi} \tan^{-1}\left(\frac{x - x_0}{a}\right) \tag{5}$$

where, x_0 is the transition center, a is known as the transition parameter and the expression πa is known as the transition length. The goal of the thermal Williams-Comstock model is to determine a and x_0 of a transition for a given HAMR system set-up. As mentioned before, transition center can be evaluated using Eqn. 4. The transition parameter is evaluated using the slope equation. See [**2**] for the derivation of each quantity of the slope equation.

Demagnetizing field is known to depend on both transition center and parameter. Therefore from Eqn. 3 and Eqn. 4, it can be seen that the two unknowns, transition center and parameter are dependent on each other and cannot be solved analytically. But, if the thermal spot size of the laser used for heating is assumed to be large, then the equations can be simplified and solved analytically. For large spot size, since the thermal gradients are small, demagnetizing field can be ignored in the calculation of transition center, thus making x_0 independent of a. Also, the demagnetizing field gradient equation simplifies, which in turn simplifies the slope equation.

If the spot size is not large, then the demagnetizing field cannot be ignored. Therefore, the system of equations (Eqn. 3 and Eqn. 4) can only be solved iteratively [**3**]. In the first iteration, for a random value of a, x_0 is calculated using Eqn. 4. Then using this value of x_0, Eqn. 3 is evaluated for a. In the second iteration, this new value of a is used to determine the new x_0 and so on. The iteration continues until both x_0 and a converges to some required accuracy.

Thermal Williams Comstock Model can be applied for both longitudinal and perpendicular HAMR. Irrespective of the direction of magnetization, the transition can be considered to follow an arctangent profile. In order to solve the slope equation, the head and demagnetizing field needs to be evaluated. The field expressions for both longitudinal and perpendicular recording is explained in the following sections.

3.1. Longitudinal HAMR. In longitudinal recording, the medium is magnetized in the longitudinal direction (along the media). The set-up of a longitudinal system is shown in Fig. 4, which shows the poles of the head and the medium beneath it. The longitudinal field between the two poles magnetizes the media in the longitudinal direction. Assuming an infinitely long and wide head with a finite gap width, Karlqvist derived an analytical expression for the field intensity in the medium [**8**]. The expression for the longitudinal component of the field is given as

$$H_x(x, y) = \frac{H_0}{\pi}\left[\tan^{-1}\left(\frac{x + g/2}{y}\right) - \tan^{-1}\left(\frac{x - g/2}{y}\right)\right] \tag{6}$$

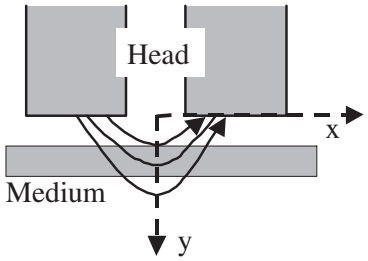

FIGURE 4. Longitudinal head and field

where g is the gap width and H_0 is the deep gap field. For the purpose of thermal Williams-Comstock model, the field is evaluated at the center of the medium. If t is the thickness of the medium and d the distance from the bottom of the head to the medium surface, then H_x is evaluated at $y = d + t/2$. The effect of the H_y component of the field is ignored in longitudinal recording. The demagnetizing field from a transition can be expressed as [**7**]

$$H_d(x) = -\frac{dM}{dx} * H_x^{\text{step}}(x) \tag{7}$$

where the field from a sharp transition at the center of the medium is given as

$$H_x^{\text{step}}(x) = \frac{1}{\pi} \tan^{-1}\left(\frac{t}{2x}\right). \tag{8}$$

Therefore, assuming an arctangent transition, the demagnetizing field can be calculated as below. If the laser spot size is large, then the demagnetizing field equation can be simplified, details of which are given in [**2**].

$$H_d(x) = \frac{-2}{\pi^2} \int_{-\infty}^{+\infty} \left[\frac{M_r(x')a}{a^2 + (x_0 - x')^2} + \tan^{-1}\left(\frac{x' - x_0}{a}\right) \frac{dM_r(T(x'))}{dx'} \right] \tan^{-1}\left(\frac{t}{2(x - x')}\right) dx' \tag{9}$$

3.2. Perpendicular HAMR. In perpendicular recording, the perpendicular field of the head magnetizes the medium in the vertical direction. The actual set-up of a perpendicular system is shown in the top of Fig 5. A highly permeable layer (or keeper) is deposited beneath the medium through which the field is conducted from one pole to the other. Note that the field is in the vertical direction in the medium. The field intensity, derived by Westmijze [**9**], is given as a complex function that needs to be solved numerically. But, by considering the equivalent system set-up (bottom of Fig. 5), an analytical head field expression can be derived [**10, 11**]. An image of the pole head can be considered to be symmetrically placed beneath the medium. When this set-up is turned sideways, the similarity with the longitudinal set-up can be readily seen. Therefore, to a good approximation the field in a perpendicular head can be evaluated using the Karlqvist expression, taking into account the change in coordinate system for the perpendicular recording. Therefore, the perpendicular component of the head field is given as

$$H_y(x, y) = \frac{H_0}{\pi} \left[\tan^{-1}\left(\frac{y + g/2}{x}\right) - \tan^{-1}\left(\frac{y - g/2}{x}\right) \right] \tag{10}$$

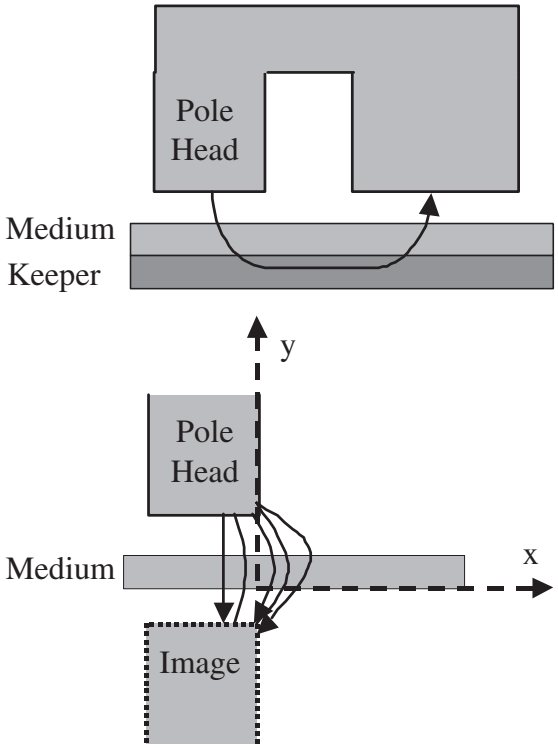

FIGURE 5. Perpendicular head and field: actual head configuration and equivalent set-up

where g is the gap width between the pole head and its image. If d is the head-medium distance and t is the medium thickness, then $g = 2d + 2t$. For the thermal Williams-Comstock model, the field is evaluated at the center of the medium ($y = t/2$). The effect of the H_x component of the field is ignored in perpendicular recording. As mentioned before, the Karlqvist expression is not a reasonable approximation for fields close to the head gap. Therefore, Eqn. 10 is valid only for $x > 0$. Since, in general, the transition occurs away from the pole edge this expression can be faithfully used in the thermal Williams-Comstock model for evaluation of transition characteristics. The demagnetizing field can be calculated using Eqn. 7, but with the perpendicular field component of a sharp transition as shown below.

$$H_d(x) = -\frac{dM}{dx} * H_y^{\text{step}}(x) \tag{11}$$

where the field from a sharp transition at the center of the medium is given as [**12**]

$$H_y^{\text{step}}(x) = \frac{1}{\pi} \tan^{-1}\left(\frac{2x}{t}\right) \tag{12}$$

Therefore, considering an arctangent transition the demagnetizing field can be calculated as,

$$H_d(x) = \frac{-2}{\pi^2}\int_{-\infty}^{+\infty}\left[\frac{M_r(x')a}{a^2+(x_0-x')^2} + \tan^{-1}\left(\frac{x'-x_0}{a}\right)\frac{dM_r(T(x'))}{dx'}\right]\tan^{-1}\left(\frac{2(x-x')}{t}\right)dx' \tag{13}$$

For a large laser spot size, the second term becomes insignificant. Consequently, the demagnetization field can be reduced to,

$$\begin{aligned} H_d(x) &\approx -\frac{2}{\pi^2}\int_{-\infty}^{\infty}\frac{M_r(x')a}{a^2+(x'-x_0)^2}\tan^{-1}\left(\frac{2(x-x')}{t}\right)dx' \\ &= \frac{2M_r(T(x))}{\pi}\tan^{-1}\left(\frac{x-x_0}{t/2+a}\right) \end{aligned} \tag{14}$$

and the gradient of the demagnetizing field can be simplified if we ignore the thermal gradient of the remnant magnetization, i.e.,

$$\frac{dH_d(x)}{dx} \approx -\frac{2M_r(T(x))}{\pi(a+t/2)} \tag{15}$$

Furthermore, similar to the derivation for longitudinal recording in [**2**], we can show that the analytical expression for the transition parameter in perpendicular recording is,

$$a = -\frac{\gamma}{2} + \frac{1}{2}\sqrt{\gamma^2 + \frac{4H_c(1-S)t}{\Delta\pi}}\Bigg|_{x_0}, \tag{16}$$

where,

$$\begin{aligned} \Delta &= \frac{dH_h}{dx} - \frac{dH_c}{dT}\frac{dT}{dx}\Big|_{x_0} = \frac{H_g g}{\pi(x_0^2+(g/2)^2)} - \frac{dH_c}{dT}\frac{dT}{dx}\Big|_{x_0}, \\ \gamma &= \frac{2M_r}{\Delta\pi} - \frac{t}{2} + \frac{2H_c(1-S)}{\Delta\pi}. \end{aligned} \tag{17}$$

4. Microtrack Model

The process of heating and magnetization of a medium is two-dimensional. But, the Williams-Comstock model provides only a one-dimensional solution to the problem of determining the transition characteristics. Therefore, they do not accurately model the magnetic transition of a track with finite width. In this section, we explain the microtrack model that closely captures the effects of this two-dimensional process. In this model, a magnetic track is divided into several sub-tracks of equal width as shown in Fig. 6. The temperature profile resulting from the heating is denoted by $T(x, y)$ where, x and y represent the directions along and across the track respectively. If N is the number of sub-tracks and Δz their width, then for each sub-track, the temperature profile is approximated by the one-dimensional function $T(x, y = i \cdot \Delta z)$, $-N/2 \le i \le N/2$. The more sub-tracks, the better the approximation. For a given system set-up, thermal Williams-Comstock model is applied independently to each of these sub-tracks to determine the corresponding transition parameter and center. If the readback response for

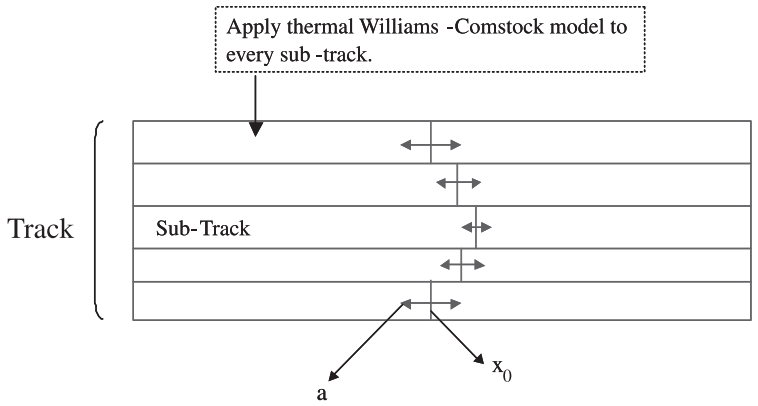

FIGURE 6. Microtrack modeling of HAMR channel

each of these sub-tracks is $h(t, a)$, then the total response of the transition is given as,

$$p(t) = \frac{1}{N} \sum_{i=1}^{N} h(t - \tau_i, a_i) \tag{18}$$

where, τ_i and a_i are the transition center and parameter of the i^{th} sub-track. The isolated transition responses for longitudinal and perpendicular recording are expressed using Lorentzian and error functions respectively [**14**].

5. Transition Characteristics

Designing a HAMR system for optimal performance is a multi-dimensional problem. The system performance is dependent not only on magnetic properties like coercivity and remnant magnetization, but also on their variation with temperature, heating profile (peak temperature, width at half of peak temperature) [**3**], and also on the position of peak temperature [**2**]. The position of the laser spot needs to be properly chosen in order to obtain the optimal performance. Since the laser is attached to the head assembly, it is not known whether it is possible to align the peak temperature with the gap center or whether it is the best possible set-up. In this section, we report on some of the unique characteristics of longitudinal HAMR induced by thermal spot.

For any system parameters, using the thermal Williams-Comstock model and the microtrack model, the transition length, location and magnetization can be determined across a track of finite width. Fig. 7 shows an example of a typical magnetization pattern of a transition in the medium for a longitudinal recording system. This figure illustrates several features of a transition that are induced by heating and are unique to HAMR. Firstly, we note that the transition occurs at different location across the track and secondly, the transition is sharp at the center and decreases progressively toward the edges of the track. Since, the thermal profile is Gaussian in both dimensions, maximum temperature occurs at the center of the track and minimum at the edges of the track. As coercivity varies linearly with

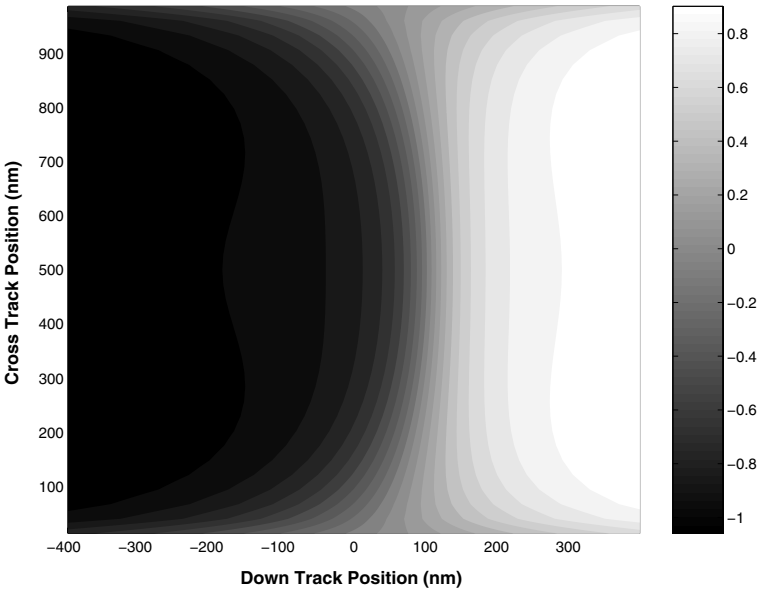

FIGURE 7. Magnetization of the medium after a transition is made

temperature, solution to Eqn. 4 varies for different sub-tracks, inducing the transition curvature across the track. The solution to transition location is a function of y, since temperature T is a function of both x and y. Thermal Williams-Comstock model suggests that high coercivity gradient induces sharper transitions. Since, coercivity gradient along the track is small at the edges, we notice a significant increase in transition length near the edges. From Eqn. 4, we note that the transition location also depends on the head field. Fig. 8 shows the shift in transition location with respect to the gap center at various deep gap fields for a system with $H_c(x,y) = -500 \cdot T(x,y) + 5 \cdot 10^5$ A/m and $M_r(x,y) = -300 \cdot T(x,y) + 3 \cdot 10^5$ A/m. It also clearly shows the transition curvature across the track.

One of the most important quantity that determines the storage capacity of HAMR is the width of the readback signal of its transitions. The width when measured at half their peak value is denoted by PW_{50} and is commonly used for purpose of comparison. Smaller the PW_{50}, greater the storage capacity of the disk. Therefore, it is necessary to investigate the effects of thermal profile on readback signal width. In the following analysis we assume a high coercive material, where $H_c(x,y) = -2000 \cdot T(x,y) + 1.6 \cdot 10^6$ A/m and $M_r(x,y) = -1200 \cdot T(x,y) + 1.2 \cdot 10^6$ A/m. Other system parameters are shown in Table 1. Fig. 9 shows the PW_{50} of the readback signal at various peak temperatures for different deep gap fields. In general, higher temperatures lead to smaller PW_{50}, but show signs of saturating or even increasing at very high temperatures. Though not shown here, this phenomenon is more pronounced with low coercive materials. For a given head field, there is an optimal temperature that achieves minimum PW_{50}. Since, higher temperatures result in lower coercivity, it is natural to expect PW_{50} to be better at high temperatures, but the reason for their saturation or increase at very high temperatures is not obvious.

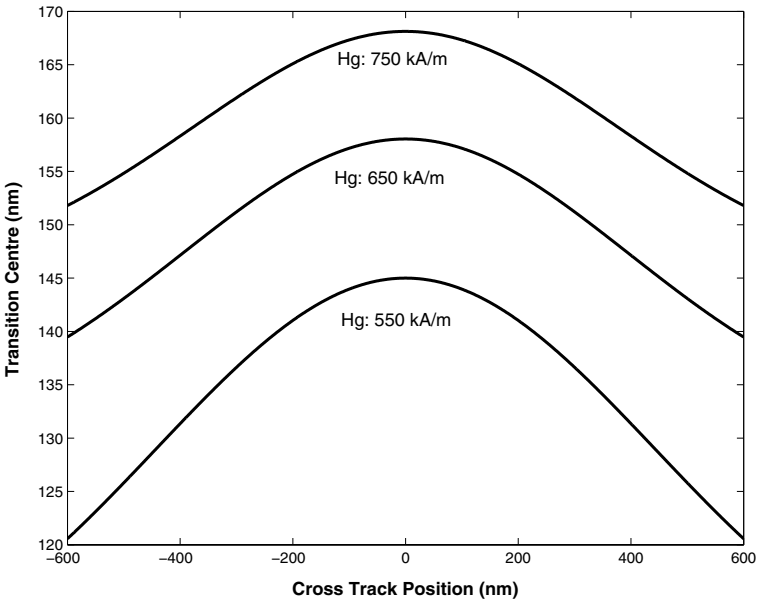

FIGURE 8. Transition center curvature across the track for various deep gap fields. For this system, $H_c(x,y) = -500 \cdot T(x,y) + 5 \cdot 10^5$ A/m and $M_r(x,y) = -300 \cdot T(x,y) + 3 \cdot 10^5$ A/m

The readback width not only depends on the peak temperature, but also on the position of the laser (or consequently the position of the peak temperature) with respect to the head gap. Along the track, the laser can be positioned either in the direction of the head movement (up-track or +X) or opposite to it (down-track or -X). For all cases, the laser is assumed to be at the center of the track in the cross-track direction. Positioning anywhere else is undesirable and is not discussed in this paper. Fig. 10 shows the PW_{50} for the same system as before with peak temperature 350 °C, at different laser spot positions around the head gap center (0 nm). Minimum PW_{50} occurs when the laser is positioned just to the right of the gap center. Moving the laser away from the gap in either direction, greatly increases the readback signal width, though it seems to decrease after reaching a peak for down-track laser spot positions. To explain such a behavior needs careful investigation. Without a proper understanding of the source of these changes, it will be difficult to generalize the behavior of any HAMR system, which has many degrees of freedom for optimization. In the following analysis, we identify the reasons for such changes and argue that it is indeed a general behavior of HAMR with high coercive materials.

The two parameters that determine the PW_{50} of the readback signal of a transition are the transition curvature of the track and parameter of each sub-track. Changing the position of the laser not only changes the temperature profile but also the coercivity of the medium. Consequently, it alters both the transition center and parameter. Fig. 11 shows an example of how the head field and the coercivity look at different laser spot positions along the down-track direction. Observe that the point of intersection of coercivity and head field is different at different laser spot

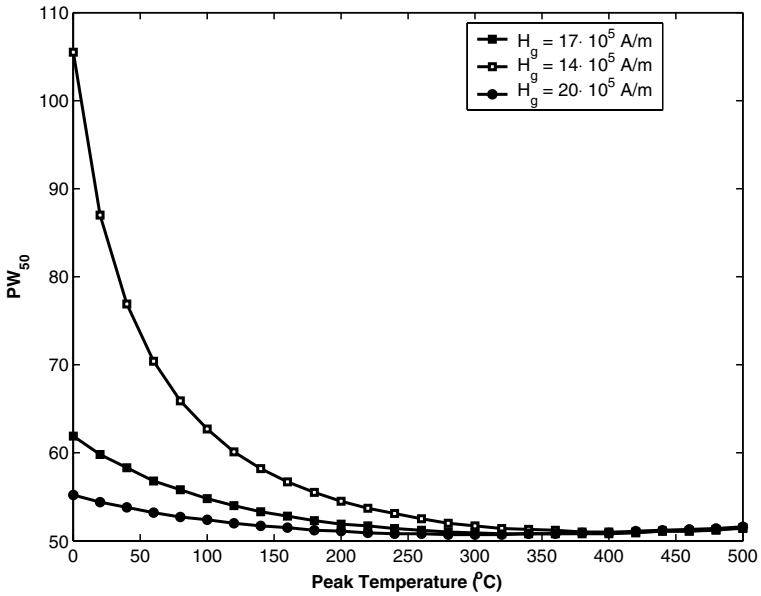

FIGURE 9. Readback signal width at various peak temperatures for different gap fields

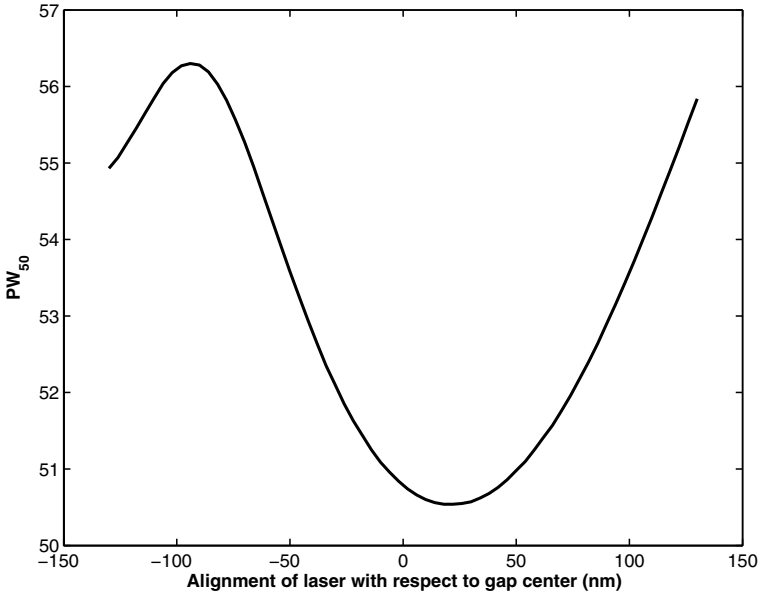

FIGURE 10. PW_{50} at various laser spot positions in Longitudinal HAMR

TABLE 1. System Parameters

Full-width half-max of laser spot	70 nm
Write head gap	100 nm
Distance from pole to medium	20 nm
Read head gap	5 nm
Width of the track	160 nm
Number of microtracks	23

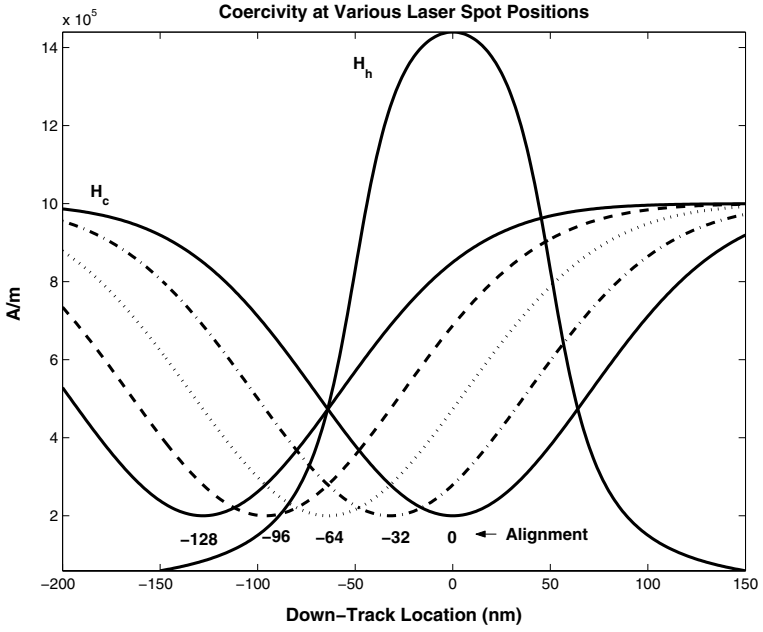

FIGURE 11. Coercivity for various laser spot positions

positions. This figure is a one-dimensional illustration of how the coercivity changes with laser spot, i.e. it is an illustration for one of the sub-tracks.

Fig. 12 shows the transition centers across the track at different laser spot positions in the down-track direction. It reveals two general trends. As the laser is moved down-track from the gap center, transition location initially move away from the gap center until they occur at the positive coercivity gradient region. Thereafter, moving the laser further down-track, moves the location back closer to the gap center. As the transition location moves away from the gap center, the curvature deteriorates, since the center now occurs closer to the peak temperature, where the variation in thermal gradient *across* the track is the highest. Consequently, in this example, the transition curvature is at its worst when the laser is aligned at around -96 nm (location closest to peak temperature) and improves on either side of this position. Fig. 13 shows the cross-track transition parameter profile for the same down-track laser spot positions. As before, two trends are identified. The parameter generally increases when laser is moved down-track toward the lower

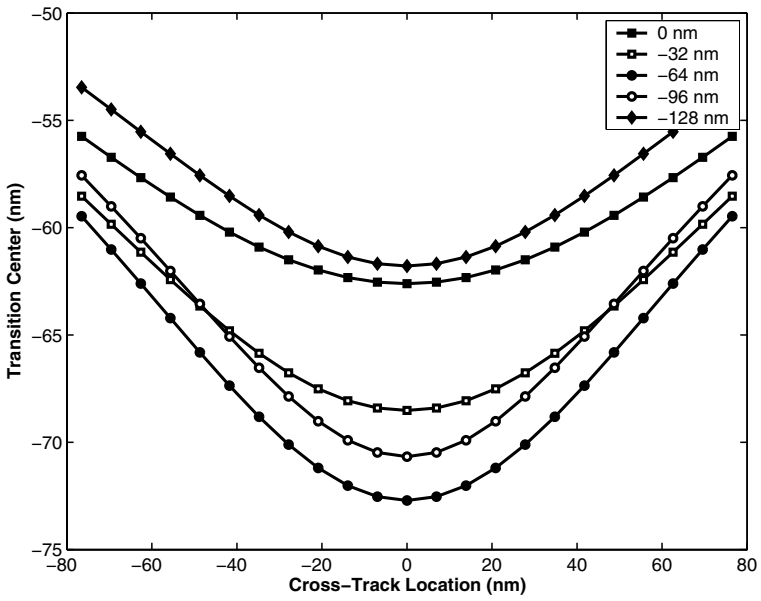

FIGURE 12. Transition centers *across* the track at various laser spot positions in the down-track direction

gradient region. In the figure, at an alignment of -96 nm there is a huge increase largely contributed by almost-zero coercivity gradient and low head field. If the transition location occurs when both coercivity gradient and head field gradient are positive, then higher coercivity gradient would result in a higher transition parameter. Since, coercivity gradient decreases toward track edges, we observe that the parameter at the center of the track increases much faster than the parameter at the edges of the track, when laser is moved down-track. At an alignment of -128 nm, though the parameter at the center remains higher than at the edges, its values have improved on account of better head field gradient at the transition location.

When laser is moved up-track, the coercivity gradient is always negative at the transition location. Also, farther the laser is from the gap center, farther the transition location is from the peak temperature. Therefore, as shown in Fig. 14, there is almost no curvature for positions far to the right of the gap center. For the same reason, as shown in Fig. 15, the change in transition parameter is almost identical throughout every sub-track. However, since the transition location is pushed to the lower temperature regions, where the coercivity gradients are smaller, transition parameter increases. PW_{50} is directly proportional to the transition parameter and is inversely proportional to the extent of curvature. If the transition location of the sub-tracks of a track are misaligned, then their combined readback response will be much wider than the response of a track whose sub-track locations are aligned with each other. As the laser is positioned along the down-track direction, PW_{50} will increase on account of deteriorating curvature though the transition parameter will be less. It will peak when the transition location occurs, where the temperature of the medium is maximum. As the laser is positioned along the up-track direction, PW_{50} will increase on account of increasing

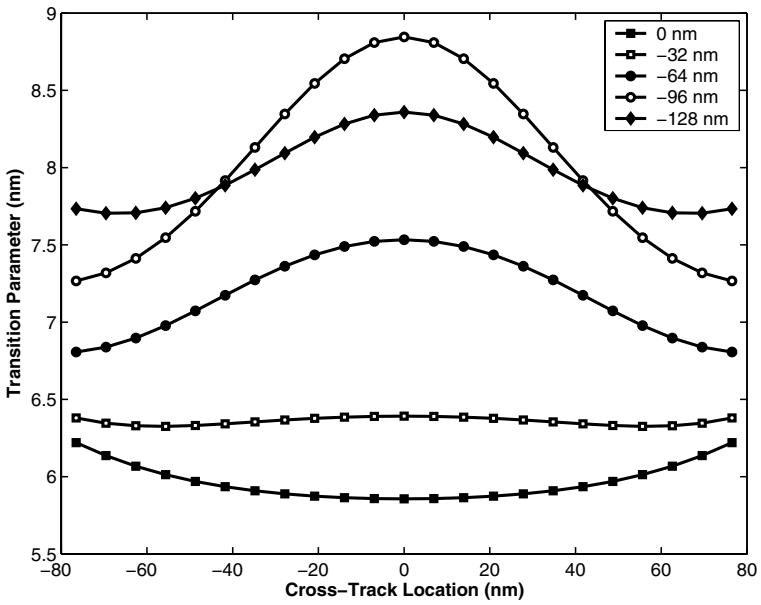

FIGURE 13. Transition parameter *across* the track at various laser spot positions in the down-track direction

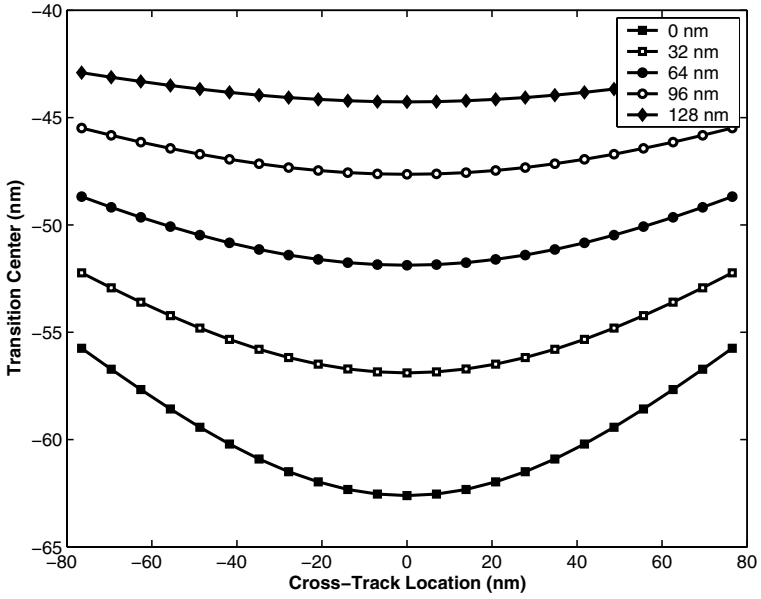

FIGURE 14. Transition centers *across* the track at various laser spot positions in the up-track direction

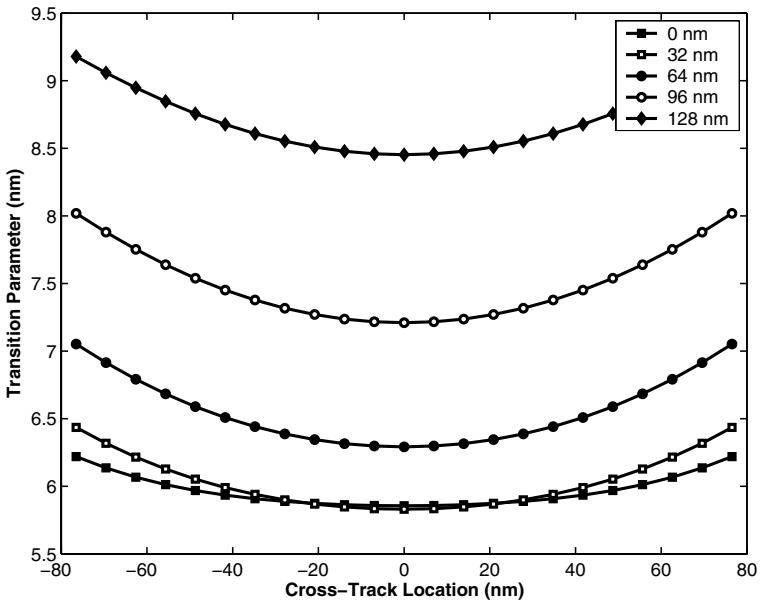

FIGURE 15. Transition parameters *across* the track at various laser spot positions in the up-track direction

transition parameter, though the curvature will improve. The minimum PW_{50} can be obtained for laser spot alignments close to the gap center. This explains the behavior observed in Fig. 10.

6. Conclusion

In this paper we introduced the thermal Williams-Comstock model for both longitudinal and perpendicular heat-assisted recording. Using this model and the microtrack model, several characteristics of HAMR were illustrated. Specifically, the effects of peak temperature and laser spot alignment on the readback response were discussed. By analyzing the underlying effects it had on the transition length and location, we identified the general system behavior to changes in thermal profile.

References

[1] M. H. Kryder, "Future trends in magnetic storage technology", *Joint NAPMRC*, Digest of Technical Papers, p. 68, Jan. 2003.

[2] T. Rausch, "Thermal Williams-Comstock model for predicting transition length in a heat-assisted magnetic recording system", *IEEE Trans. Mag.*, vol. 40, no. 1, pp. 137–147, Jan. 2004.

[3] M. F. Erden, T. Rausch and W. A. Challener, "Cross-track location and transition parameter effects in heat-assisted magnetic recording", *IEEE Trans. Mag.*, vol. 41, no. 6, pp. 2189–2194, June 2005.

[4] T. W. McDaniel and W. A. Challener, "Issues in design of media for hybrid recording", *Trans. Magn. Soc. Jpn.*, vol. 2, pp. 316–321, 2002.

[5] T. W. McDaniel, W. A. Challener and K. Sendur, "Issues in heat-assisted perpendicular recording", *IEEE Trans. Mag.*, vol. 39, no. 4, pp. 1972–1979, Jul. 2003.

[6] W. A. Challener, T. W. McDaniel, C. Mihalcea, K. Mountfield, K. Pelhos and K. Sendur, "Light delivery techniques for heat-assisted magnetic recording", *Jpn. J. Appl. Phys.*, vol. 42, pp. 981–988, 2003.
[7] S. X. Wang and A. M. Taratorin, *Magnetic Information Storage Technology*, Academic Press, 1999.
[8] O. Karlqvist, "Calculation of magnetic field in the ferromagnetic layer of a magnetic drum", *Trans. Roy. Inst. Tech.*, no. 86, 1954.
[9] W. K. Westmijze, "Studies on magnetic recording", *Phillips Res. Rep.*, part II, vol. 8, no. 3, & Part III, vol. 8, no. 4, 1953.
[10] J. C. Mallinson and H. N. Bertram, "On the characteristics of pole-keeper head fields", *IEEE Trans. Mag.*, vol. 20, no. 5, pp. 721–723, Sept. 1984.
[11] J. C. Mallinson and H. N. Bertram, "A theoretical and experimental comparison of longitudinal and vertical modes of magnetic recording", *IEEE Trans. Mag.*, vol. 20, no. 3, pp. 461–467, May 1984.
[12] H. N. Bertram, *Theory of Magnetic Recording*, Cambridge University Press, 2003.
[13] Y. Zhang and H. N. Bertram, "A theoretical study of nonlinear transition shift", *IEEE Trans. Mag.*, vol. 34, no. 4, pp. 1955–1957, July 1998.
[14] B. Vasic and E. M. Kurtas, *Coding and Signal Processing for Magnetic Recording Systems*, chapter 18, pp. 18.1-18.12, CRC Press, 2004.

Department of Electrical and Computer Engineering, University of Arizona, Tucson, Arizona 85721
E-mail address: rathna@ece.arizona.edu

Department of Electrical and Computer Engineering, University of Arizona, Tucson, Arizona 85721
E-mail address: vasic@ece.arizona.edu

Seagate Research, Pittsburgh, Pennsylvania 15222
E-mail address: fatih.erden@seagate.com

Seagate Research, Pittsburgh, Pennsylvania 15222
E-mail address: ching.he@seagate.com